Flexible Weaving Constructed Self-Powered Pressure Sensor Enabling Continuous Diagnosis of Cardiovascular Disease and Measurement of Cuffless Blood Pressure

Keyu Meng, Jun Chen, Xiaoshi Li, Yufen Wu, Wenjing Fan, Zhihao Zhou, Qiang He, Xue Wang, Xing Fan, Yuxin Zhang, Jin Yang,* and Zhong Lin Wang*

Pulse wave carries comprehensive information regarding the human cardiovascular system (CS), which is essential for directly capturing CS parameters. More importantly, cuffless blood pressure (BP) is one of the most critical markers in CS. Accurately measuring BP via the pulse wave for continuous and noninvasive diagnosis of a disease associated with hypertension remains a challenge and highly desirable. Here, a flexible weaving constructed self-powered pressure sensor (WCSPS) is reported for measurement of the pulse wave and BP in a noninvasive manner. The WCSPS holds an ultrasensitivity of 45.7 mV Pa^{-1} with an ultrafast response time of less than 5 ms, and no performance degradation is observed after up to 40 000 motion cycles. Furthermore, a low power consumption sensor system is developed for precisely monitoring pulse wave from the fingertip, wrist, ear, and ankles. A practical measurement is performed with 100 people with ages spanning from 24 to 82 years and different health statuses. The discrepancy between the measured BP results using the WCSPS and that provided by the commercial cuff-based device is about 0.87–3.65%. This work demonstrates an efficient and cost-effective way for human health monitoring, which would be a competitive alternative to current complex cardiovascular monitoring systems.

1. Introduction

With the rapid development of modern society, science and technology, the tempo of life is becoming more and more intense. Real-time heath monitoring and assessment is becoming more and more critical and indispensable, which largely contributes to the advancement of the field of wearable electronics for biomedical applications,[1–5] and may open up the individual-centered disease diagnosis. Pulse wave, as one of the most representative signals in human bodies, carries comprehensive information regarding human cardiovascular system (CS), which is highly correlated with various physiological diseases. Variations in pulse wave waveform are also important basis for evaluating the physiological and pathological status of human CS.[6–8] Continuous and noninvasive health measurement realizes the idea of real-time pulse wave monitoring, which has a crucial effect for early prevention of hypertension and improving treatment efficiency. To measure the subtle changes in the pulse wave, traditional techniques are the cuff type and focused on the Korotkoff sound method or oscillometric method, which are largely shadowed by structure complexity, fabrication of high-quality materials, reliance on external power source, and poor portability and scalability.[9,10] Besides, blood pressure (BP) measurement with an arterial catheter is considered to be the most standard and accurate method, but its invasive nature has several disadvantages.[11–13] In addition, the cuff will object pressure onto the arm or wrist position, and the applied tension can cause errors and lead to

Dr. K. Meng, X. Li, W. Fan, Z. Zhou, Q. He, X. Wang, Y. Zhang,
Prof. J. Yang
Department of Optoelectronic Engineering
Key Laboratory of Optoelectronic Technology and Systems
Ministry of Education
Chongqing University
Chongqing 400044, P. R. China
E-mail: yangjin@cqu.edu.cn
Dr. J. Chen
Department of Materials Science and Engineering
Stanford University
Stanford, CA 94305, USA

Dr. J. Chen, Prof. Z. L. Wang
School of Materials Science and Engineering
Georgia Institute of Technology
Atlanta, GA 30332, USA
E-mail: zhong.wang@mse.gatech.edu
Dr. Y. Wu
College of Physics and Electronic Engineering
Chongqing Normal University
Chongqing 400044, P. R. China
Dr. X. Fan
College of Chemistry and Chemical Engineering
Chongqing University
Chongqing 400044, P. R. China
Prof. Z. L. Wang
Beijing Institute of Nanoenergy and Nanosystems
Chinese Academy of Sciences
Beijing 100083, P. R. China

the discomfort of user. In the meanwhile, various novel materials and technologies are applied to develop wearable sensors over the past decades, including photoplethysmography,[14–16] ultrasound wall-tracking technique,[17–19] carbon nanotube,[20–22] piezoelectric materials,[23–26] metal nanowires,[27–30] and conductive fibers.[31–34] However, the reported wearable sensors are incapable of measuring the distinguishable dynamic pressure patterns of pulse wave owing to the insufficient sensitivity.
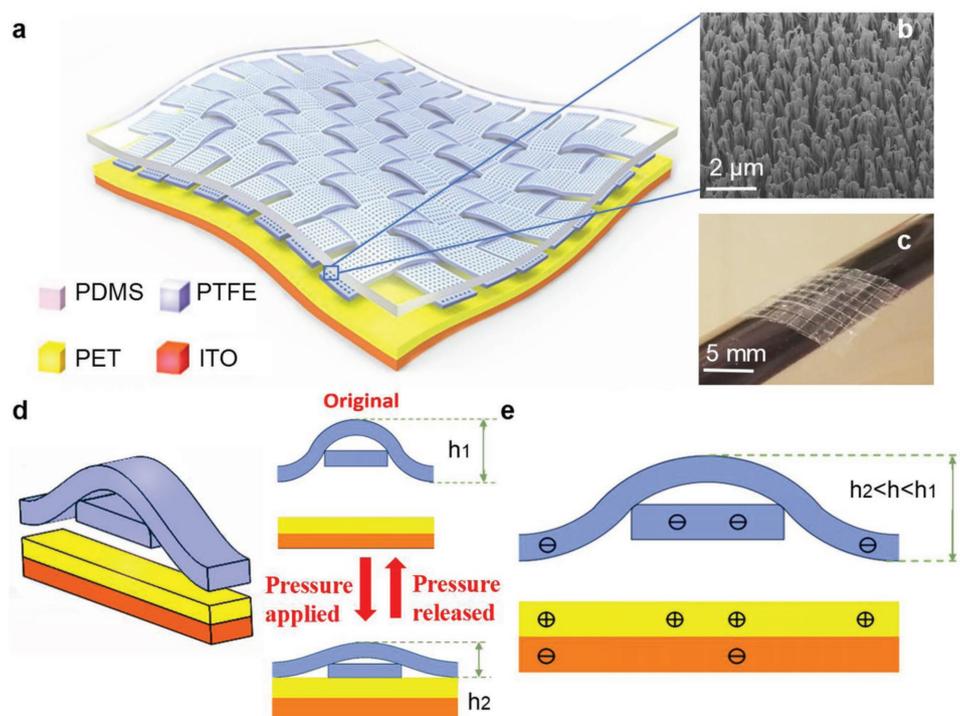
Besides, continuous monitoring of the physiological parameters always requires adhesive electrodes and connecting wires, which may cause patients uncomfortableness and inconvenience for operation surgery. This brings a major obstacle to the wider application in market. As a consequence, utilizing a noninvasive user-friendly method to continuously monitor the human pulse wave and wirelessly transmit the results to personal electronics is a highly desired approach to realize dynamic and real-time health care as well as prevention of cardiovascular disease in daily life.

Here, we developed a weaving constructed self-powered pressure sensor (WCSPS) for continuous measurement of human pulse wave velocity (PWV) and BP. Relying on the rational weaving structure design and plasma etching to create surface polymer nanowires, the designed device exceeds in capturing and conversing the subtle blood pressure change into electrical signals for cardiovascular disease prevention and diagnosis. With an unprecedentedly fast response time of less than 5 ms,[35–38] the WCSPS holds an excellent sensitivity of 45.7 mV Pa^{-1}. And no performance degradation was observed after 40 000 cycles' continuous operation. Additionally, a further step was taken to develop a cost-effective, wearable, user-friendly, and low power consumption sensor system, which includes a WCSPS for human pulse signal extraction, a signal management circuit for signal processing, and a wireless transmission component to communicate the measured cardiovascular parameters to personal mobile phone for continuous human health monitoring. The low power consumption sensor system is capable of extracting real-time weak pulse signals from human carotid, fingertip, ankle, and ear with excellent stability, which enabled us to realize the precise measurement of PWV and BP from various body positions. Owing to the high sensitivity of the WCSPS and wide adaptability of the genetic algorithm (GA), the discrepancy between the measured BP results by WCSPS and OMRON device is only about 0.87–3.65%. In the meanwhile, the wireless transmitting to personal electronics assures that the measured health data are easily accessible to user. Via a system-level optimization, all the system components can collaboratively work together for continuous and noninvasive human health assessment and monitoring with no restrictions on time and place.

2. Results and Discussion

The WCSPS holds a multilayer structure as schematically shown in **Figure 1**a, which was inspired the common textile for clothes with traditional woven patterns.[39–42] The WCSPS,

Figure 1. A WCSPS for self-powered measurement of human PWV and BP. a) Schematic illustration of the flexible weaving constructed self-powered pressure sensor. b) A SEM image of plasma-etched PTFE nanowires. The scale bar is 2 µm. c) A photograph showing an as-fabricated WCSPS, which is flexible, lightweight, and can be easily wrapped onto a curved surface. The scale bar is 5 mm. d) Schematic diagram of the cross-sectional view of a single unit of the WCSPS. The right side illustrates the two conditions that when the device is in its original state (h_1) and when the external pressure was applied (h_2). e) An illustration showing the electrical signal generation process of the WCSPS.

**ADVANCED
SCIENCE NEWS**
www.advancedsciencenews.com
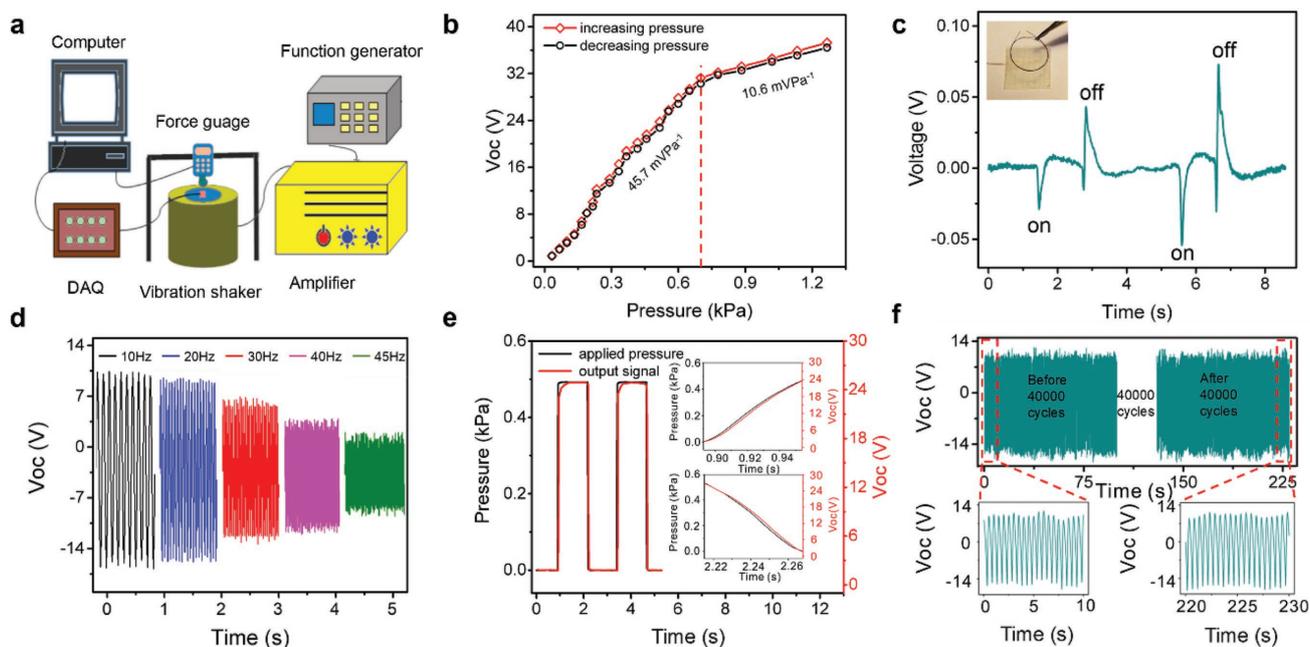
**ADVANCED
FUNCTIONAL
MATERIALS**
www.afm-journal.de

with a thickness of 1 mm and scalable dimensions, is flexible, wearable, and even foldable. On the bottom, a layer of polyethylene terephthalate (PET) acts as one electrification layer with indium–tin oxide (ITO) as the back electrode. Then, a layer of polytetrafluoroethylene (PTFE) strips with interlaced woven structure was placed above the PET substrate, acting as another electrification layer. Notably, the dimension of each stripe is 8 mm × 1.3 mm. Finally, a polydimethylsiloxane (PDMS) thin film with a thickness of 70 μm was used as a protective layer outward on the top of the interlaced PTFE strips. In order to improve the output performance of WCSPS, vertically aligned polymer nanowires were created onto the PTFE surface via plasma etching for an intimate contact with PET. A scanning electron microscopy (SEM) image of PTFE nanowires is displayed in Figure 1b, which indicates that the average clustering diameter of nanowires is about 110 nm with an average length of 0.8 μm. The nanowire-enhanced surface roughness, on one hand, is capable of improving the surface triboelectrification and inducing a larger triboelectric charge density for higher electrical signal output. On the other hand, the created nanowires can be easily deformed for higher measurement sensitivity to external subtle mechanical excitation. Additionally, without PTFE nanowires, the contact between the PET and PTFE is not compact at certain points due to the surface morphology and structures, as illustrated in Figure S1 (Supporting Information). It is worth noting that the pressure sensitivity with nanomaterials' modification is improved to about 1.4 times of that of the WCSPS without nanomaterials' surface modification. As a result, the polymer nanowire structure of PTFE can result in an improvement of the effective contact area and higher pressure sensitivity. As demonstrated in Figure 1c, a photograph shows an as-fabricated WCSPS, which is flexible, lightweight, and can be easily wrapped onto a curved surface. Inspired by an interlaced weaving structure, the working principle of the WCSPS can be elucidated from two aspects, namely, pulse-induced membrane vibration and vibration-induced electrical signal generation. On one hand, as sketched in Figure 1d, it shows the cross-sectional view of a single unit of the WCSPS. The right side illustrates two mechanical states: when the device is in its original state (h_1) and when the external pressure is applied (h_2). In the original state, the PTFE strips separate from PET thin film (Figure 1d, top right). When the pulse pressure brings the PTFE to fully contact with PET, the largest distance between the two will be shortened to $h = h_2$. During this processing, the effective contact area between the two triboelectric layers will increase (Figure 1d, bottom right). On the contrary, when the applied pressure is released, the contact area at the crisscross intersection will gradually return to its original state. The charge distribution is shown in Figure 1e. At the same time, the distance will also between the range of h_1 and h_2. It is worth noting that the weaving construction here is a critical point to fabricate the sensor with high sensitivity. To compare, the mechanical deformation patterns in response to external pressure (0.01 N) of the PTFE layers respectively with and without woven structure were simulated by a finite element analysis, as shown in Figure S2 (Supporting Information).

On the other hand, the changing of the effective contact area at crisscross intersection from mechanical states h_1 to h_2 will induce an electric potential difference owing to a coupling between contact electrification and electrostatic induction. Since PET is much more triboelectrically positive than PTFE, thus PTFE is more likely to grab electrons and PET tends to give them up at the interface of contact. As a result, negative charges are accumulated on the PTFE side and positive ones are aggregated on the PET side. A fully cycle of the working mechanism of WCSPS was schematically demonstrated in Figure S3 (Supporting Information). In addition, the surface charge potential distributions with and without woven structure were also simulated by COMSOL in three dimension, as shown in Figure S4 (Supporting Information). Additionally, the open-circuit voltage of the WCSPS without the weaving construction under external pressures was shown in Figure S5 (Supporting Information). It can be found that there exists a lower pressure sensitivity without the weaving construction under both increasing and decreasing applied pressures compared with the WCSPS, especially in the low-pressure region. Thus, the weaving constructed PTFE in the WCSPS plays an important role of promoting the pressure sensitivity. It revealed that the woven structure will greatly boost the effective contact area and electric signals, which is improved to about 1.64 times of that without woven structure. In addition, the dependence of the output voltage on the number of the stripes was also studied and shown in Figure S6 (Supporting Information), which indicated that the electric output will increase with elevation of the stripes in the woven structure. Thus, the WCSPS is scalable for mass production as wearable devices.

To characterize the performance of the WCSPS, a customized pressure testing system was developed with a vibration table and high-precision force gauge, as illustrated in **Figure 2**a. At the constant frequency of 2 Hz, the dependence of WCSPS electrical output on the applied pressures was continuously measured with gradually increasing the pressure then decreasing back to zero, as demonstrated in Figure 2b. The concrete time profiles of open-circuit voltage, short-circuit current under different pressures, are presented in Figure S7 (Supporting Information). The forward and backward voltage–pressure curves show little hysteresis with an error less than 3.4%. It is worth noting that the pressure response of the device holds two distinct slope regions. In the lower-pressure (<0.71 kPa) region, voltage increases linearly till the applied pressure of 0.71 kPa, indicating a pressure sensitivity of 45.7 mV Pa^{-1}. Then the increasing of voltage with elevation of applied pressure slows down, indicating a lower pressure sensitivity of 10.6 mV Pa^{-1}. A limited detectable pressure as small as 2.5 Pa was observed, as shown in Figure S8 (Supporting Information). For the bending test, repeated bending/relaxation cycles (angles ranging from 5° to 30°) were applied to the WCSPS, and the open-circuit voltage fluctuates within 3 V, as shown in Figure S9 (Supporting Information).

To further verify the high sensitivity of the sensor to external pressure, a human hair with the weight of 5 mg was gently picked up or dropped onto the WCSPS within an area of 1 cm^2, and a 0.06 V voltage was thus generated, as demonstrated in Figure 2c. Furthermore, in order to verify the high-frequency response characteristics of the WCSPS, we measured the open-circuit voltage of the WCSPS under pressure with the frequency ranging from 10 to 45 Hz, as shown in Figure 2d. It can be seen that the sensor still maintains stable output under the
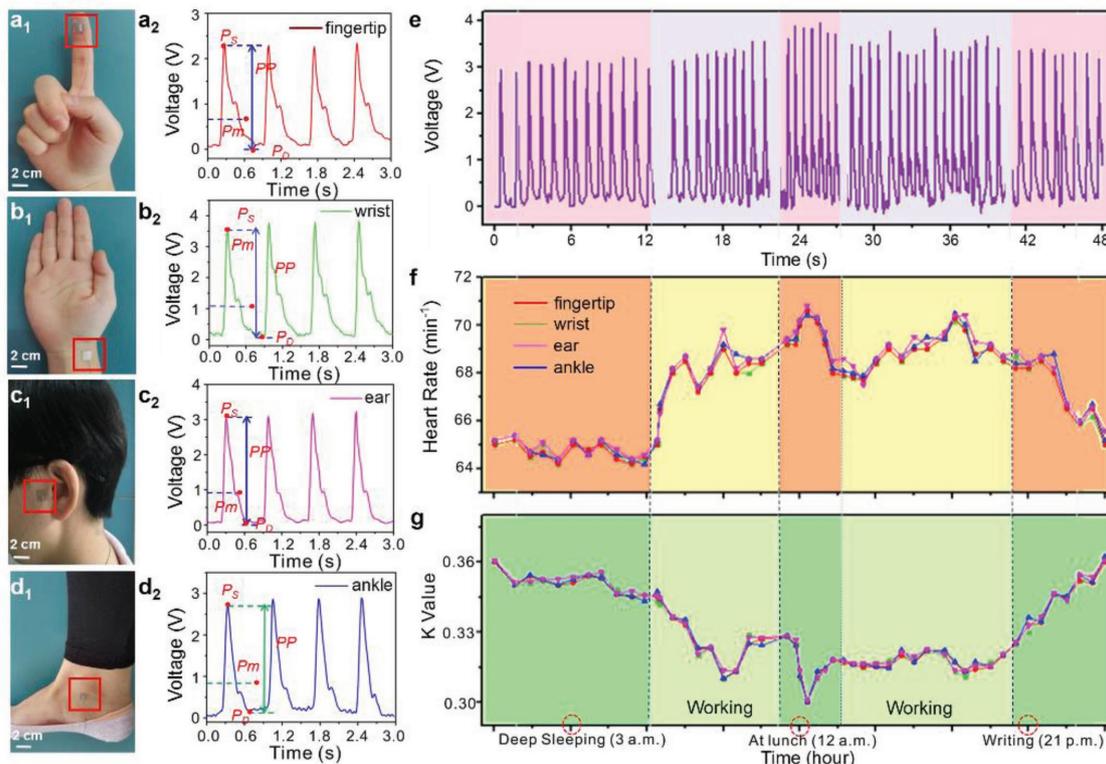
Figure 2. Electrical output and mechanical robustness measurements of the WCSPS. a) Schematic diagram of the experimental testing setup. b) The continuous electrical output of the WCSPS in response to the continuously applied external pressure in a measurement cycle. c) The pulse sensor is able to sense the even tiny pressures. The data were acquired when a 5 mg hair was placed and removed from the WCSPS. d) The V_{oc} was tested by periodically applying the pressure under higher frequencies of 10, 20, 30, 40, and 45 Hz, respectively. e) WCSPS response time characterization. The response time was tested by periodically applying the pressure. Two insets are the enlarged view of the rising and falling edges of a period, indicating a response time less than 5 ms. f) Device mechanical robustness investigation. There is no observable performance degradation.

excitation with high frequency to 45 Hz, and the V_{oc} gradually decreased with increasing frequency. Thus, the WCSPS is not only suitable for the measurement of low-frequency signals, but can also guarantee the stable output for higher-frequency signals. In addition, to measure the sensor response time, the output voltage signals under dynamic pressure inputs were characterized and shown in Figure 2e. The time profile of sensor output voltage is well overlapped with that of the applied pressure. An enlarged view of the time profile in the loading and unloading process in one operation cycle indicates an ultrafast response time of less than 5 ms, which would enable its wide-range practical applications, such as electronic skin.

As a sensor, the device robustness and output stability are also very important for practical applications. To evaluate it, the WCSPS was continuously tested under a pressure of 0.6 kPa at a frequency of 2 Hz. And during the 40 000 loading/unloading cycles, output voltages of the first and the last 200 cycles were respectively recorded, as shown in Figure 2f. For a detailed comparison, the enlarged views of output waveform in the first and last 10 s were also presented, and no performance degradation was observed. In addition, a further step was taken to evaluate the device performance after ≈40 000 cycles' operation. The output signals do not show significant hysteresis with the increasing/decreasing pressure, as shown in Figure S10 (Supporting Information). These results indicate that the WCSPS holds a decent mechanical robustness and stability for practical applications.

Owing to the ultrasensitivity and fast response time, the WCSPS is capable of capturing detailed information of dynamic change in human blood vessels for further real-time noninvasive PWV and BP measurements. Technically, the arterial pulse can be perceived directly from the skin surface, such as fingertips, wrist, neck, ankle, ear, and other parts. However, the pulse signals are relatively weaker at the finger and ankle part than that at human ear and wrist. With a low detection limit and high sensitivity, the WCSPS is capable of extracting most of the pulse wave from most parts of the human body. As shown in **Figure 3**a_1-d_1, the device was worn against different human body, including fingertips, wrist, ear, and ankle. The measured pulse waveforms were respectively shown in Figure 3a_2-d_2. In this paper, we use noninvasive WCSPS to measure the pulse waves at the superficial arteries. In this case, the amplitude of the pressure waves at superficial in different body parts is related to many factors, such as the supportive bony structure or the thick tissue, and so on. Thus, the output voltages of the WCSPS worn against different human body parts are varied. Besides, we carried out an experiment to validate the measurement consistency on different vessel positions in the same body part. As shown in Figure S11a (Supporting Information), the center of the WCSPS was worn against the seven vessel positions of the wrist for pulse wave monitoring. The corresponding measured pulse waveforms were, respectively, shown in Figure S11b–h (Supporting Information). It can be seen that, for all the vessel positions except the position f, the critical characterization points of the pulse waveforms can be captured precisely and no enormous waveform distortion was observed. The changes of cardiovascular physiology and pathology will cause the change of the characteristic and the area of the pulse transit map, which can be reflected in the change of the K value of the characteristic quantity.[43] Namely, the K value renders the

Figure 3. Demonstration of the WCSPS for human pulse measurement. a_1–d_1) Photographs showing that the WCSPS was directly worn at the fingertip, wrist, ear, and ankle, respectively. a_2–d_2) Photographs are respectively the measured electrical signals from the four places. e) The measured electrical signals, f) heart rate, g) the K value of the participants at different times of the day, including deep sleeping, at lunch, and night writing. Here, the K value is defined as $K = (P_m - P_d)/(P_s - P_d)$. P_m is the mean arterial pressure, P_s is the systolic peak, and P_d is the diastolic valley points.

degree of vascular sclerosis, and it is an important physiological indicator of cardiovascular clinical examination. Reliance on the characterization points in the acquired pulse waveform, the K value can be calculated as

$$K = \frac{P_m - P_d}{P_s - P_d} \tag{1}$$

where $P_m = \frac{1}{T}\int_0^T p(t)\,dt$ is the mean arterial pressure, T is the cardiac cycle, P_s is the systolic peak, and P_d is the diastolic valley point. It can be seen that K value is determined only by the shape of the pulse wave rather than the absolute value of systolic and diastolic blood pressure (SBP and DBP), corresponding to the percentage of the mean value of the pulsating wave pressure pulsation components to the maximum of the pulsating components. Various physiological and pathological states of the pulse waveform and area will lead to the pulse waveform changes, which can be evaluated by the K value. Owing to the WCSPS's superior sensitivity to the external subtle pressure change, the critical characterization points of the pulse waveform, including P_s, P_d, and P_m, can be well captured and measured. As a result, the K values can be calculated, and were respectively obtained from fingertips (0.319), wrist (0.314), ear (0.316), and ankle (0.315). These values can well evaluate the physiological and pathological states of human CS. The systolic and diastolic pulse waves in the human arterial system are not only subjected to the human heart itself,

but also to the flowing situations at all levels of the artery and its branches with various physiological factors. Reliance on the obtained K value, the cardiovascular physiological parameters, artery compliance (AC) and total peripheral resistance (TPR), can be calculated according to the following equations[43,44]
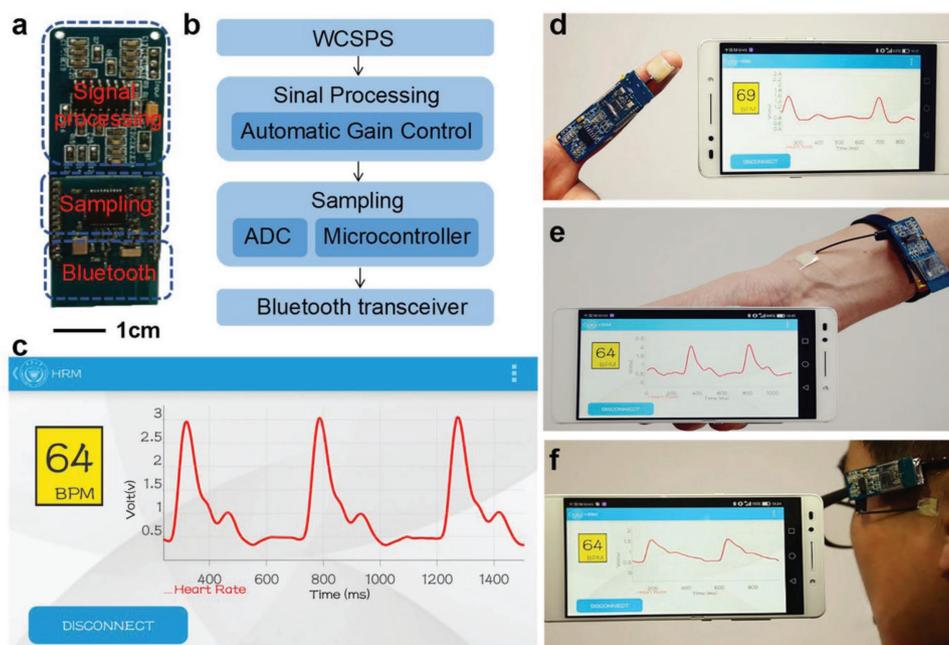
$$AC = \frac{SV}{P_s - P_d} \tag{2}$$

$$TPR = \frac{P_m}{SV} \times T \tag{3}$$

where stroke volume $SV = \frac{0.28}{K^2}(P_s - P_d)T$ (mL). All the parameters P_s, P_d, HR, and K, can be easily measured noninvasively and continuously by the WCSPS. When the peripheral resistance, vascular elasticity, and blood viscosity get changes, K value, AC, and TPR will have a corresponding change. During the practical experiment, it was found that the different physiological conditions sometimes have the same K value, while AC and TPR varied. Thus, only calculating K value is not enough to assess the characteristics of cardiovascular system completely. Therefore, we calculated K value, AC, and TPR simultaneously, which can help us to evaluate the health status of cardiovascular system more accurately and prevent the cardiovascular diseases timely. For practical demonstration of continuous human health monitoring, Figure 3e shows a real-time pulse waveform

**ADVANCED
SCIENCE NEWS**
www.advancedsciencenews.com

**ADVANCED
FUNCTIONAL
MATERIALS**
www.afm-journal.de

of an individual during the time slot of 1 day. In order to characterize the pulse waveform at different time periods clearly, we separated the acquired pulse wave data into five segments corresponding to the five motion states of the participant, respectively. In Figure 3e, several consecutive period pulse waveforms were displayed in each segment. Three typical time periods, including deep sleeping, at lunch and night writing, were, respectively, selected for the pulse waveform extraction. The detail drawing of the waveforms is shown in Figure S12 (Supporting Information). Based on the acquired pulse wave signals, the corresponding calculated K value and heart rate are presented in Figure 3f and Figure 3g, respectively. The average heart rate was recorded every 0.5 h. For each recording, 10 min pulse signal data were used to calculate the average of the heart rate. It can be clearly seen from the results' statistic that heart rate is lower during the deep sleeping stage. For lunch time, the heart rate increased significantly, while it slightly decreased for the participant writing at night. A distinct change of parameters is mainly attributed to that, when people under exercise load, it will result in the decreasing of TPR and K value and increase of AC due to the muscle expansion movement. However, the value will be increased after a period of rest. The three parameters could well reflect the cardiovascular health conditions of the human body. With the change of physiological factors such as peripheral vascular resistance and the degree of hardening of the blood vessel wall, there will be a series of regular changes in the characteristics of the pulse wave of the human body, so that the K value will also change accordingly, which can be seen from Figure S13a,b (Supporting Information), the recorded real-time voltages over several pulse periods with WCSPS being placed over the wrist of a 25 year old and a 70 year old woman.

Furthermore, in order to verify the capability of measuring the pulse wave of obese subject, we carried out a supplementary experiment, as shown in Figure S14a (Supporting Information). The measured carotid artery pulse wave of the obese subject (158 cm, 95 kg, 52 year old woman) was plotted in Figure S14b (Supporting Information). Owing to the ultrasensitivity of WCSPS, the critical characterization points of the pulse waveform can be well captured and measured precisely although the obese subject with thick tissue. It shows great promising and can realize the long-term continuous diagnostics.

As an individual sensor, the WCSPS is capable of capturing subtle mechanical change in the blood pressure in the vessel and expressing it in electrical signals as human pulse waveform. A further step was taken to develop a user-friendly sensor system for human heart rate monitoring. It includes the WCSPS for human pulse signal extraction and signal management circuits, respectively, for pulse signal processing and wireless data transmission to personal electronics. As a product of system-level optimization, all the system components collaboratively work together for real-time human health monitoring. A photograph of signal management circuit was shown in **Figure 4**a. Figure 4b shows a schematic diagram of the signal management circuit. The normal heartbeat rate for an adult is typically ≈1–5 Hz, and the optimized signal processing specially designed to remove the interference data from lower-frequency body movements as well as environment noises for more precisely detecting the human pulse waveform. A sampling rate of 500 Hz was utilized. Here, the acquired raw pulse wave signal from the WCSPS was first processed by an automatic gain control (AGC). The recommended operating conditions of the amplifier chip and filter chip were listed in Figure S15

Figure 4. The developed low power consumption sensor system for human heart rate monitoring, which is a product of system-level optimization, including a WCSPS for human pulse signal extraction and a signal management circuit for signal processing and transmission. a) Photograph of the as-developed signal management circuit. b) A schematic diagram of the signal management circuit. c) A real-time pulse wave was displayed on a commercial cell phone via APP interface for human heart rate monitoring. Photographs showing that the low power consumption sensor system is worn against d) human finger, e) wrist, f) ear for real-time pulse wave measurement. The real-time data can be received and displayed on mobile phone APP.

(Supporting Information). Then, the signals were collected via an analog-to-digital conversion (ADC). ADC module converted the analog pulse signal into a digital signal. High-precision 12 bits ADC and appropriate sampling rate ensure the synchronous data acquisition with abundant details. Followed by conditioning and signal sampling is a microcontroller unit (MCU), with the capability of computing and serial communicating precisely, MCU plays a critical role of calibrating the acquired signals for further data processing. Then the processed digital signals were sent to the mobile phone via the Bluetooth module. After a series of data manipulation, the processed signal was transmitted to the mobile phone terminal application (APP) by means of Bluetooth technology. Figure 4c demonstrated that a real-time pulse wave was displaying on a commercial cell phone via APP interface for human heart rate monitoring. To prove the capability of the low power consumption sensor system for noninvasive arterial pulse measurement, it was placed directly on finger, wrist, and ear three parts, and the measured data can be received and displayed in mobile phone APP in a real-time manner. Figure 4d–f shows that the low power consumption sensor system is worn against human finger (Movie S1, Supporting Information), wrist (Movie S2, Supporting Information), and ear (Movie S3, Supporting Information) for real-time pulse wave measurement. The real-time data can be received and displayed on mobile phone APP. Featured as being compact, wireless, lightweight, and high sensitivity, the WCSPS-based low power consumption sensor system provides an efficient and cost-effective alternative to current expensive healthcare facilities such as hospitals or nursing homes.

Since the noninvasive and real-time continuous BP measurement is critical for the prognosis and diagnosis of cardiovascular diseases, medically, aortic PWV is considered as the effective and reproducible method to measure the BP via conventional blood pressure cuff measurement device. The PWV highly relies on the physical conditions, thickness, and diameter of the arterial wall. The PWV can reflect the arterial elasticity and compliance. A larger PWV value means a worse arterial elasticity and higher arterial stiffness, which can be calculated via the Moens–Korteweg equation[45]

$$PWV = \frac{d}{PTT} = \sqrt{\frac{Eh}{2\rho r}} \tag{4}$$

where d represents the propagation distance of the pulse wave. PTT is the time interval between the maximum value of epidermal pulse wave in different parts of each cardiac cycle being determined, E is the elastic modulus of vessel wall, h is the thickness of the blood vessel, r is the arterial radius, and ρ is the blood density.
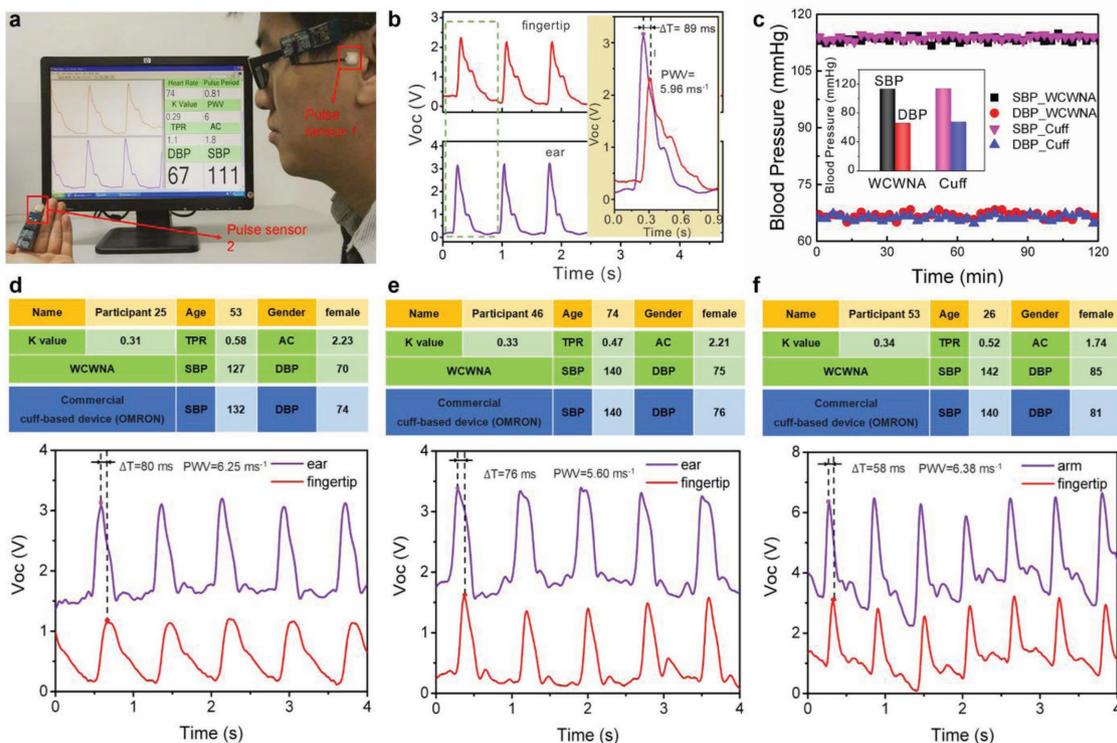
For a same individual, the elasticity of blood vessels will not change greatly in a short period of time. It has been proved that the PTT has a strong correlation with BP, and this relation is highly dependent to each individual physiological properties. Therefore, linearizing the logarithmic model can be expressed as[46]

$$BP = aPTT + b \tag{5}$$

where a and b are the undetermined coefficients, and the value varies from individual to individual.

In the previous work for BP measurement, it requires mass statistics to estimate coefficients a and b, which is not convenient for real-time monitoring BP. To alleviate this issue, in our study, the GA was proposed to calculate the BP in a real-time manner. GA is an efficient global search algorithm based on natural selection and genetic theory, which combines the survival rule of the fittest in the process of biological evolution with the random information exchange system within the group. GA abandons the traditional search method but simulates the process of natural biological evolution and uses artificial evolution to search the target space randomly. More details about the generic algorithm were demonstrated in Nota S1 (Supporting Information).

To demonstrate the capability of the wearable low power consumption sensor system for a real-time BP measurement, two identical sensor systems were respectively worn against over fingertip and ear to detect human pulse waves, as shown in **Figure 5**a; the results were spontaneously read from the personal electronics (Movie S4, Supporting Information). The systems were connected to NI DAQ (NI PCI 6251) by means of wire connection, and then, the acquired signals can be displayed in real time and saved in personal computer by Labview programming. Owing to the high time resolution of the NI PCI 6251 (50 ns), the signals of the two sensors can guarantee strict synchronization for accurate PTT and BP calculating. The measured pulse waveforms were presented in Figure 5b. The PTT was determined by measuring the signal time delay between the two pulse waves. Then, the output signal was amplified under a cycle period, as shown in the enlarged view. It is worth noting that a 89 ms time delay was observed between the peak point of the signal acquired from fingertip and that of from the ear. A PWV = 5.96 ms^{-1} from fingertip to ear was obtained by this experiment. Furthermore, we used the improved GA algorithm to calculate the BP in a real-time manner. In the GA algorithm, the important point is that we select the K value as a constraint condition to track the dynamic changes of the BP without a mass of regression data. As shown in Figure 5c, SBP and DBP values are calculated during a 2 h continuous monitoring, and the results are well consistent with the values obtained from the conventional photoplethysmogram (PPG)/electrocardiogram (ECG)[47,48] technique. Furthermore, compared to the average values of the SBP and DBP with the readings provided by an electronic sphygmomanometer from OMRON (an intelligent electronic sphygmomanometer which is easy to operate, economical and practical), our PWV-based method provides an SBP of 130.1 ± 2.5 mmHg and a DBP of 63.5 ± 2.3 mmHg (inset in Figure 5c), while the cuff-based OMRON device provides an SBP of 128.8 ± 1.6 mmHg and a DBP of 64.3 ± 1.8 mmHg. It indicates that the measurement in this work is as accurate as the results from current commercial BP measuring devices. Furthermore, to prove the practicality of the wearable low power consumption sensor system for noninvasive continuous biomedical monitoring, a practical measurement of the cardiovascular parameters (K, TPR, AC, and BP values) was carried out at a community hospital. We randomly selected 100 participants with ages spanning from 24 to 82 years old with different health status. For each participant, we first used our sensor system to measure the BP. Then, in order to verify the accuracy of BP measurement, a cuff-based sphygmomanometer (OMRON) was

Figure 5. The low power consumption sensor system for quantitatively measuring the human PWV and BP. a) The photograph showing that the low power consumption sensor system was simultaneously monitoring the pulse waves from human fingertip and ear, and real-time reads out the PWV and BP values of the participant. b) The real-time extracted voltage signals when the sensor system was working at human finger and ear. An enlarged view of the voltage signal in a pulse cycle for real-time PWV measurement. c) Systolic blood pressure (SBP) and diastolic blood pressure (DBP) measurements. The real-time health monitoring of d) middle-aged and aged people, e) hypertensive patients, and f) pregnant women.

used to test the BP of the same participant. Based on the test results, we divided them into five groups according to the difference of age and the health status (including 11 young people, 57 middle-aged and aged people, 10 participants with hypertensive, 15 pregnant women and 7 pregnant women with high blood pressure). Figure 5d–f shows the recorded real-time pulse waves over several pulse periods and the calculated results of the K, TPR, AC, and BP for three participants, respectively, including middle-aged and aged people, hypertensive patients, and pregnant women. The rest of the participants with different health status are shown in Figures S16–S69 (Supporting Information). A statistical result of the cardiovascular parameters is shown in **Table 1**. From the test results in Table 1, the cardiovascular health status of the middle-aged and aged people was better than that of the hypertensive patients but worse than that of the young people. The cardiovascular parameters of elderly (60–75 year old) in group B are similar to the middle-aged (38–60 year old) participants. While the cardiovascular parameters of the elderly in group C were poor than the elderly in group B. With the increase of the blood pressure, the K value and TPR increased, and the AC value decreased. The measured results are consistent with the human physiological characteristics. These three parameters independently but complementarily indicate the stiffness of the arteries, that is, the increase of K value and TPR represents the increasing of arterial stiffness, while the AC values followed a reverse trend upon arterial stiffness, which are especially accurate for hypertensive people.

Moreover, there is a slight discrepancy, about 0.87–3.65%, between the measured BP results by WCSPS and that provided by the commercial cuff-based device. These statistical results highlight that the measured waveform by WCSPS can not only

Table 1. Results of the cardiovascular health parameters for 100 participants. ("A" denotes young people with ages spanning from 24 to 29 years old; "B" denotes middle-aged and aged people with ages spanning from 38 to 75 years old; "C" denotes hypertensive patients; "D" denotes pregnant women with high blood pressure; "E" denotes healthy pregnant women; SBP monitoring discrepancy = |SBP$_{WCSPS}$ − SBP$_{cuff-based}$|/SBP$_{cuff-based}$ × 100%; DBP monitoring discrepancy = |DBP$_{WCSPS}$ − DBP$_{cuff-based}$|/DBP$_{cuff-based}$ × 100%).

	A	B	C	D	E
K value	0.29	0.31	0.32	0.32	0.28
TPR	0.61	0.77	0.87	0.57	0.51
AC	3.04	2.55	2.46	1.79	2.39
SBP by WCSPS	109	114	151	141	116
DBP by WCSPS	68	73	93	85	78
SBP by cuff-based device	107	112	154	139	115
DBP by cuff-based device	67	71	95	82	77
SBP measurement discrepancy	2.01%	1.79%	1.95%	1.43%	0.87%
DBP measurement discrepancy	1.84%	1.41%	2.11%	3.65%	1.29%

**ADVANCED
SCIENCE NEWS**

www.advancedsciencenews.com

**ADVANCED
FUNCTIONAL
MATERIALS**

www.afm-journal.de

reflect the CS condition but also be utilized for noninvasive and real-time continuous BP measurement.

3. Conclusions

In this work, we first developed a WCSPS for capturing subtle mechanical change of the blood pressure in the vessel and expressing it in electrical signals as human pulse waveform. Featured with an excellent sensitivity of 45.7 mV Pa^{-1} in a wide detection range of ≈710 Pa, the WCSPS holds a low pressure detection limit of 2.5 Pa, a fast response time less than 5 ms, and a small scale of $10 \times 10 \times 1$ mm^3 for ease in carrying. It is capable of self-powered and continuous measurement of human pulse wave and BP. Still, the device has a good mechanical robustness, and no performance degradation was observed after 40 000 cycles' continuous operation. In addition, based on the WCSPS, a low power consumption sensor system was further developed, including a WCSPS for human pulse signal extraction, a management circuit for signal processing and a wireless transmission component to communicate the measured cardiovascular parameters to personal mobile phone. Via a system-level optimization, all the components can collaboratively work together and the measured results are as accurate as the results from current commercial BP measuring devices. This work paved a simple, cost-effective, and user-friendly approach for low power consumption measuring human PWV and BP, which would be a competitive alternative to current complex cardiovascular monitoring systems and could be immediately and extensively adopted in a variety of applications, and ultimately improving our way of living.

4. Experimental Section

Fabrication of Nanowires Array on PTFE Surface: A PTFE film with 25 μm thickness was cleaned subsequently by menthol, isopropyl alcohol, and deionized water. Then, the inductively coupled plasma (ICP) reactive-ion etching was used to fabricate the aligned nanowires on the PTFE surface. O$_2$, Ar, and CF$_4$ gases were injected into the ICP chamber with flow ratios of 10.0, 15.0, and 30.0 sccm, respectively. A large density of plasma was produced by a power source of 400 W. 100 W was used to accelerate as another power source of the plasma ions. The obtained PTFE nanowires had an average length of ≈0.8 μm for about 60 s continuous etching.

Fabrication of a WCSPS: 1) A layer of 100 nm ITO was deposited on one side of PET as electrode. Then the layer of PET (thickness 75 μm) was cut into square shapes with an area of ≈1 cm^2. 2) The dimension of all the stripes was 8 mm × 1.3 mm, and they were woven into a kirigami pattern. 3) The kirigami pattern layer was put on the PET side with ITO-coated side. 4) The fabricated PDMS film was cut into the same size with PET and then it was covered onto the kirigami pattern layer with anchored four corners.

Experimental Setup for Pressure Measurement: A 3D vibration table was employed for the WCSPS pressure sensor characterization. First, two flat sheets were, respectively, anchored onto the vibration table and the pressure gauge, and the WCSPS was sandwiched between the two surfaces for an accurate measurement. An electrometer was utilized to monitor and record the sensor output, and thus the applied pressure. In the meanwhile, the applied pressure was increased and decreased gradually and the output signals were recorded to investigate the dependence of voltage on different applied pressures.

Experimental Setup for the Electrical Signal Measurement: For the dynamic force measurement and electrical signal extraction, a computer-based user interface, a function generator (Stanford DS345) and an amplifier (LabworkPa-13) were systematically involved. A digital Force Gauges (DSM-2) was also employed to measure the external pressure. All participants provided informed consent to participate in the experiments for the verification of the accuracy of the blood pressure measurements and for the publication of the data and any accompanying identifiable images.

Supporting Information

Supporting Information is available from the Wiley Online Library or from the author.

Conflict of Interest

The authors declare no conflict of interest.

[1] F. Yi, X. Wang, S. Niu, S. Li, Y. Yin, K. Dai, G. Zhang, L. Lin, Z. Wen, H. Guo, J. Wang, M.-H. Yeh, Y. Zi, Q. Liao, Z. You, Y. Zhang, Z. L. Wang, *Sci. Adv.* **2016**, *2*, e1501624.

[2] Y. Lai, J. Deng, S. Zhang, S. Niu, H. Guo, Z. L. Wang, *Adv. Funct. Mater.* **2017**, *27*, 1604462.

[3] X. Pu, H. Guo, J. Chen, X. Wang, Y. Xi, C. Hu, Z. L. Wang, *Sci. Adv.* **2017**, *3*, e1700694.

[4] P. Yang, L. Lin, F. Yi, X. Li, K. C. Pradel, Y. Zi, C. Wu, J. He, Y. Zhang, Z. L. Wang, *Adv. Mater.* **2015**, *27*, 3817.

[5] X. Y. Fan, Y. Huang, X. R. Ding, N. Q. Luo, C. L. Li, N. Zhao, S.-C. Chen, *Adv. Funct. Mater.* **2018**, 1805045.

[6] J. Yang, J. Chen, Y. Su, Q. Jing, Z. Li, F. Yi, X. Wen, Z. Wang, Z. L. Wang, *Adv. Mater.* **2015**, *27*, 1316.

[7] C. M. Boutry, A. Nguyen, Q. O. Lawal, A. Chortos, S. Rondeau-Gagné, Z. Bao, *Adv. Mater.* **2015**, *27*, 6954.

[8] X. Han, X. Chen, X. Tang, Y. Chen, J. Liu, Q. D. Shen, *Adv. Funct. Mater.* **2016**, *26*, 3640.

[9] K. Wichman, G. Rydén, M. Wichman, *Acta Obstet. Gynecol. Scand.* **1984**, *63*, 25.

[10] R. E. Climie, M. G. Schultz, S. B. Nikolic, K. D. Ahuja, J. W. Fell, J. E. Sharman, *Am. J. Hypertens.* **2012**, *25*, 414.

[11] M. T. Ganter, J. A. Alhashemi, A. M. Al-Shabasy, U. M. Schmid, P. Schott, S. A. Shalabi, A. M. Badri, S. Hartnack, C. K. Hofer, *J. Clin. Monit. Comput.* **2016**, *30*, 13.

[12] T. Shiba, T. Mao, R. Hashimoto, T. Matsumoto, Y. Hori, *Graefe's Arch. Clin. Exp. Ophthalmol.* **2016**, *254*, 1195.

[13] K. Lakhal, S. Ehrmann, T. Boulain, *Chest* **2017**, *4*, 1023.

[14] C.-C. Chuang, J.-J. Ye, W.-C. Lin, K.-T. Lee, Y.-T. Tai, *J. Clin. Monit. Comput.* **2015**, *29*, 801.

[15] A. A. Kamshilin, I. S. Sidorov, L. Babayan, M. A. Volynsky, R. Giniatullin, O. V. Mamontov, *Biomed. Opt. Express* **2016**, *7*, 5138.

[16] Z. Marcinkevics, M. Greve, J. I. Aivars, R. Erts, A. H. Zehtabi, *Acta Univ. Latviensis* **2009**, *753*, 59.

[17] J. Seo, S. J. Pietrangelo, H. S. Lee, C. G. Sodini, *IEEE Trans. Ultrason., Ferroelectr., Freq. Control.* **2015**, *62*, 776.

[18] A. G. Miller, A. J. Bardin, *Respir. Care* **2016**, *61*, 383.

[19] C. H. Wang, X. S. Li, H. J. Hu, L. Zhang, Z. L. Huang, M. Y. Lin, Z. R. Zhang, Z. N. Yin, B. Huang, H. Gong, S. Bhaskaran, Y. Gu, M. Makihata, Y. X. Guo, Y. S. Lei, Y. M. Chen, C. F. Wang, Y. Li, T. J. Zhang, Z. Y. Chen, A. P. Pisano, L. F. Zhang, Q. F. Zhou, S. Xu, *Nat. Biomed. Eng.* **2018**, *561*, 516.

[20] O. Kanoun, C. Müller, A. Benchirouf, A. Sanli, T. R. Dinh, A. Al-Hamry, L. Bu, C. Gerlachand, A. Bouhamed, *Sensors* **2014**, *14*, 10042.

[21] L. Cai, L. Song, P. Luan, Q. Zhang, N. Zhang, Q. Gao, D. Zhao, X. Zhang, M. Tu, F. Yang, W. Zhou, Q. Fan, J. Luo, W. Zhou, P. Ajayan, S. Xie, *Sci. Rep.* **2013**, *3*, 3048.

[22] S. Park, M. Vosguerichian, Z. Bao, *Nanoscale* **2013**, *5*, 1727.

[23] K. Park, M. Lee, Y. Liu, S. Moon, G. Hwang, G. Zhu, J. E. Kim, S. O. Kim, D. K. Kim, Z. L. Wang, K. J. Lee, *Adv. Mater.* **2012**, *24*, 2999.

[24] Y. K. Fuh, J. Ye, P. C. Chen, H. C. Ho, Z. M. Huang, *ACS Appl. Mater. Interfaces* **2015**, *7*, 16923.

[25] K. Shin, J. Lee, J. Jang, *Nano Energy* **2016**, *22*, 95.

[26] R. Bao, C. Wang, L. Dong, R. Yu, K. Zhao, Z. L. Wang, C. Pan, *Adv. Funct. Mater.* **2015**, *25*, 2884.

[27] J. Lee, S. Kim, D. Yang, B. C. Park, S. Ryu, I. Park, *Nanoscale* **2014**, *6*, 11932.

[28] Y. Cheng, R. Wang, J. Sun, L. Gao, *ACS Nano* **2015**, *9*, 3887.

[29] B. Hwang, J. Lee, T. Q. Trung, E. Roh, D. Kim, S. Kim, N. Lee, *ACS Nano* **2015**, *9*, 8801.

[30] S. Hong, H. Lee, J. Lee, J. Kwon, S. Han, Y. D. Sun, H. Cho, J. Shin, J. Yeo, S. H. Ko, *Adv. Mater.* **2015**, *27*, 4744.

[31] J. Chen, Z. L. Wang, *Joule* **2017**, *1*, 480.

[32] J. Chen, Y. Huang, N. N. Zhang, H. Y. Zou, R. Y. Liu, C. Y. Tao, X. Fan, Z. L. Wang, *Nat. Energy* **2016**, *1*, 16138.

[33] Y. Wei, S. Chen, X. Yuan, P. Wang, L. Liu, *Adv. Funct. Mater.* **2016**, *26*, 5078.

[34] J. Ge, L. Sun, F. Zhang, Y. Zhang, L. Shi, H. Zhao, H. Zhu, H. Jiang, S. Yu, *Adv. Mater.* **2016**, *28*, 722.

[35] X. Wang, Y. Gu, Z. Xiong, Z. Cui, T. Zhang, *Adv. Mater.* **2014**, *26*, 1336.

[36] S. Gong, W. Schwalb, Y. Wang, Y. Chen, Y. Tang, J. Si, B. Shirinzadeh, W. Cheng, *Nat. Commun.* **2014**, *5*, 3132.

[37] J. Lee, H. Kwon, J. Seo, S. Shin, J. H. Koo, C. Pang, S. Son, J. H. Kim, Y. H. Jang, D. E. Kim, T. Lee, *Adv. Mater.* **2015**, *27*, 2433.

[38] G. Y. Bae, S. W. Pak, D. Kim, G. Lee, D. H. Kim, Y. Chung, K. Cho, *Adv. Mater.* **2016**, *28*, 5300.

[39] N. Zhang, J. Chen, Y. Huang, W. Guo, J. Yang, J. Du, X. Fan, C. Tao, *Adv. Mater.* **2016**, *28*, 263.

[40] X. Pu, L. Li, M. Liu, C. Jiang, C. Du, Z. Zhao, W. Hu, Z. L. Wang, *Adv. Mater.* **2016**, *28*, 98.

[41] T. Zhou, C. Zhang, C. Han, F. Fan, W. Tang, Z. L. Wang, *ACS Appl. Mater. Interfaces* **2014**, *6*, 14695.

[42] J. Chen, Y. Huang, N. Zhang, H. Zou, R. Liu, C. Tao, X. Fan, Z. L. Wang, *Nat. Energy* **2016**, *1*, 16138.

[43] J. Song, S. Zhang, Y. Qiao, Z. Luo, J. Zhang, Y. Zeng, L. Wang, *Eur. J. Obstet. Gynecol. Reprod. Biol.* **2004**, *117*, 162.

[44] D. Chemla, J. Hébert, C. Coirault, K. Zamani, I. Suard, P. Colin, Y. Lecarpentier, *Am. J. Physiol.: Heart Circ. Physiol.* **1998**, *274*, H500.

[45] C. J. Bramwell, A. V. Hill, *Proc. R. Soc. B* **1922**, *93*, 298.

[46] Y. Yoon, J. H. Cho, G. Yoon, *J. Med. Syst.* **2009**, *33*, 261.

[47] W. Chen, T. Kobayashi, S. Ichikawa, Y. Takeuchi, T. Togawa, *Med. Biol. Eng. Comput.* **2000**, *38*, 569.

[48] Y. Heravimohammadamin, M. Keivan, J. Sima, *Int. J. Comput. Appl.* **2014**, *103*, 36.

1806388 (10 of 10)